USE OF UAV DATA IN MAPPING AND MANAGEMENT MINING AND ENVIRONMENTAL OPERATIONS IN QUARRIES

Raquel Sofia da Cruz Morais[1]

[1]*Instituto Superior Técnico, Universidade de Lisboa, Portugal* – raquelmorais@tecnico.ulisboa.pt

ABSTRACT

Unlike so many other sectors, where the advantages of using Unoccupied Aerial Vehicles (UAVs) have already been thoroughly exploited, when we talk about the extractive industry, more expensive, time-consuming and less secure traditional surveys still prevail. The low cost combined with high accuracy and remarkable efficiency in time enable UAVs to become a reliable procedure of data acquisition in the extractive industry, serving as a support tool in 3D modeling, distance and volume calculations, and geological and environmental monitoring.

In this dissertation will be evaluated the capacity of the use of UAV data as a tool to support the operations of the extractive industry, such as the development of the topographic surveys of the quarry to support the monitoring and planning of the dismantling, the 3D inventory of the disassembled material and aggregate piles, as well as the extraction of the drainage network and the study of the impact of dust on surrounding vegetation. The quality of these products with and without control points will be also evaluated together with the comparison of volumes estimation with mathematical models and actual weights.

The proposed study involves the capture of images using an UAV, the collection of coordinates on the ground with a GNSS receiver, the processing of data and the creation of photogrammetric products, namely, point clouds, orthophotos and digital surface models. It was concluded that the use of UAV data in the extractive industry allows optimizing processes with greater agility and precision, enabling strategic planning of decisions in a faster way, as well as monitoring and recording the temporal activities.

KEYWORDS: unoccupied aerial vehicle, UAV, quarry mapping, quarry operations management, environmental management

1. INTRODUCTION

The constant search for increased productivity in unit operations and the reduction of production costs stimulates the development and improvement of tools and methods that help decision-making in the work routines of the various sectors of the production process of the mineral industry, from the planning of activities, through the optimization of unit operations inherent to the mineral production cycle , until it reaches the monitoring of the environment and the rehabilitation of the area degraded by extractive activity (Vasconcelos et al., 2018).

Unlike so many other sectors, where the advantages of using UAVs have already been thoroughly exploited, when we talk about the extractive industry, the most time-consuming and sometimes risky traditional security surveys still prevail, requiring many readings of the terrain for accurate modulation and measurement of it. Although the conventional method was the most used in the characterization of rocky masses in quarries, the use of photogrammetry using UAVs has proven reliable and effective, thanks to its accessibility, speed and relative low investment cost, allow the acquisition of data that serve as a support tool in 3D and topographical modeling survey of terrain, calculations of distances and measurement of volumes and geological and environmental monitoring (Salvini et al., 2017; Aguilera et al., 2012).

In this context, the main motivation for the development of this dissertation is the detailed evaluation of technological innovation in the use of a multirotor UAV to perform the topographic survey of an open pit quarry to map the quarry and generate productivity gains, contributing to a better planning and management of the quarry.

Partner company in the study

This work had as a study target the Casal Farto nº3 ornamental limestone quarry, operated by the company Filstone - Comércio de Rochas, S.A., as well as the surrounding area of the support infrastructure and the area of the crushing unit. The Casal Farto nº3 quarry belongs to the Casal Farto quarry nucleus (Figure 1), in Fatima, Ourém.

Figure 1: Location of Filstone- Comério de Rochas, S.A. company in the core of quarries Casal Farto.

2. MATERIAL AND METHODS

2.1. Methodology

The automatic generation of DEM from oriented and calibrated aerial image routines has been used by researchers for more than 20 years (Krzystek, 1991; Colomina & Molina, 2014), which has led to the design of a robust and well-established procedure for modern SfM digital photogrammetry. Figure 2 shows a flowchart summarizing the steps performed from data acquisition to obtaining the final product.

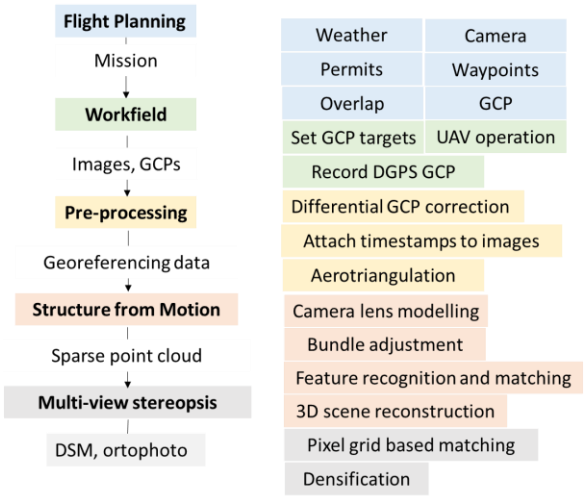

Figure 2: Workflow from data acquisition to obtaining the final product

Before starting the 3D reconstruction process, it's necessary to preprocessing the working block, in which the photos captured during the flight are added, the project output coordinate system is defined, the blurred photographs are removed, and the corresponding characteristic points are identified between the images. In this initial stage, aerotriangulation is used, a process of research of conjugated points in different photographs, which will increase the network of support points in the block, to know in each photograph the coordinates of the terrain. These points will serve as a link between photographs and adjacent scans, called tie points. The geometric and positional accuracy of the project can be optimized by the insertion of georeferenced GCPs (Ground Control Points) in this step.

The 3D reconstruction process is possible due to the creation of the Computational Technique Structure from Motion (SfM). The term SfM is derived from the expression structure derived from a moving sensor, which occurs in view of the need for a large amount of image taking in different positions and with high overlap between them, for the three-dimensional reconstruction of a scene (Micheletti et al., 2015). The SfM method estimates, from the correspondence between images, the calibration of the camera in different positions, based on internal and external orientation parameters, in order to generate a sparse point cloud (Szeliski, 2010).The orientation and position of the image captured (determined by the inertial positioning system on board the UAV) as well as the calibration of the camera are determined using the Scale Invariant Feature Transform (SIFT) algorithm, which identifies homologous points in pairs of images overlapped with each other to establish a spatial correlation between the images in a three-dimensional coordinate system , resulting in an insensitive representation to variations in lighting and orientation. Next, the Sparse Bundle Adjustment procedure transforms the tie points into a three-dimensional geometric model of the scene, generating a sparse point cloud (AGISOFT LLC, 2016; Loew, 2004).

Subsequently, oriented and calibrated images are processed using Multi View Stereo (MVS) techniques, which using as input the orientation and location of the modeled camera, perform a systematic search to find the best pixels matches in all overlapping sets of key characteristic points, thus performing a matching, expansion and filtering approach, creating a dense point cloud with high level of detail of three-dimensional geometry (Harwin & Lucieer, 2012; Bemis et al., 2014).The dense point cloud is then used to reconstruct the geometry of the surface-shaped object, from which the orthophoto and the DEM can be generated (AGISOFT LLC, 2016).

2.1.1. Volume Measurement

Volume estimations are fundamental for many industries, so the ability to do so quickly and accurately is essential to ensure quality of results and cost efficiency. UAV technology is potentially an extraordinary tool for computing volumes given its flexibility, accessibility and ease of use (Raeva et al. 2016).

The Pix4Dmapper software uses the generated DSM to calculate the volume of objects, and the degree of uncertainty in the calculations depends on the spatial resolution of the GSD since it determines the accuracy with which the coordinates of each point were calculated. Pix4DMapper calculates two volumes, one Cut Volume, when the terrain is higher than the base surface, and a Fill Volume, when the terrain is below the base. Thus, the total volume is defined by the sum of these two volumes.

2.1.2. Identification of the drainage network

Topography is one of the most important factors for the formation of the direction of surface water flows and basins. Much of the analysis of hydrological patterns can be calculated from digital terrain models obtained from UAV's data processing.

The first step to determine the drainage network is to identify the direction of surface water flow. There are several methods to calculate the flow direction, and to perform this task we opted for the use D8 algorithm, one of the methods most frequently used for its algorithmic ease and understandable structure. The D8 algorithm is a method

in which the flow is determined in a single direction from largest to smallest value, between 8 neighboring cells in a 3x3 window. If a cell is smaller than its eight neighbors, that cell receives the value of its lowest neighbors, and the stream is set in the direction of that cell. By determining the flow direction of cells, you can determine the volume that seeps into each cell and calculate the cumulative flow model. After the cumulative flow model is created, you can extract the drainage network. For this, limit values of cells are defined, which will be part of the drainage network (Gunen et al., 2019).

2.1.3. Dust impact analysis

The exploitation of open pit mines and quarries affects surrounding vegetation cover, as well as soil properties and hydrological structure. The digital images captured by UAVs can be a low-cost method to evaluate and monitor the impact that the extractive industry has on vegetation, from the study of various vegetation indices, in this case derived from RGB images. However, it should be noted that these vegetation indices, once based on RGB images, have certain advantages and limitations in terms of highlighting or omission of certain surfaces. Therefore, it should be considered that the application of vegetation indices based on RGB is limited about monitoring the growth stages of the vegetation, since the most appropriate length to do so is the next infra-red (Bendig et al., 2015; Tucker, 1979).

The analysis of the different spectral responses of the vegetation allows us to generate different indices. The table 1 shows the vegetation indices tested in this dissertation.

Table 1: Vegetation Index from RGB images

Index	Formula	Reference
Modified green-red vegetation index (MGRVI)	$MGRVI = \frac{G^2 - R^2}{G^2 + R^2}$	Bending et al. (2015)
Green leaf index (GLI)	$GLI = \frac{(2 \times G) - R - B}{(2 \times G) + R + B}$	Louhaichi et al. (2001)
Red green-blue vegetation (RGBVI)	$RGBVI = \frac{G^2 - R \times B}{G^2 + R \times B}$	Bending et al. (2015)
Visible Atmospherically Resistant Index (VARI)	$VARI = \frac{G - R}{R + G + B}$	Gitelson et al. (2002)
Normalized Difference Vegetation Index (NDVI)	$NDVI = \frac{NIR - R}{NIR + R}$	Rouse et al. (1974)

To calculate the NDVI from RGB images, the equation proposed by Arai et al (2016) was used, to obtain an approximation of the Near Infrared (NIR) band:

$$NIR = \frac{R - 360.6}{-1.1941} \quad (1)$$

2.2. Equipment and Software

The UAV used in the realization of the dissertation is the Phantom 4 RTK of DJI, a quadcopter drone of aerophotogrammetric survey with high precision that combines navigation and positioning at the centimetric level to a high-performance imaging system, to significantly reduce operational difficulties and costs (DroneShow, 2018). The Phantom 4 RTK comes with a remote control with integrated display with which we can in addition to using the basic commands of drone driving, also carry out mission planning. The UAV is equipped with GPS and GNSS systems to accurately track and execute your flight routes, maintaining accurate values for distance, altitude, speed and positioning. For the imaging system, it has a 1-inch and 20 MP CMOS sensor. Due to the high resolution, the drone can reach a GSD of 2.74 cm to 100 meters of flight altitude.

The D-RTK 2 Mobile Station of DJI (Figure 3) was also used, to provide real-time differential data to the UAV, creating an accurate survey solution. The D-RTK 2 supports GNSS GPS, BeiDou, GLONASS and Galileo frequencies, offering a horizontal positioning accuracy of 1cm+1ppm (RMS) and 2cm+1ppm vertical positioning (RMS) (DJI, 2020).

Figure 3: Phantom 4 RTK (left) and D-RTK 2 (right)

During the work, three software was used. To draw the KML file polygon of the area to be mapped, to define a flight plan route, was used the Google Earth. Data processing was performed in the Pix4DMapper software, which allows creating the 3D point cloud, DSM, orthophoto, as well as possibilities for measuring distances and calculate volumes. The Software QGis was also used to extract the drainage network from the surface water and calculate the vegetation indices. Final products can also be easily imported and worked on Civil 3D software, a useful tool to support the planning and monitoring of the dismantling.

2.3. Workflow

Phase 1 – Flight Preparation

Phase 1 aims to define the area to be mapped and its application, to outline the path to the flight and define the variables that will produce the best results. To carry out the Flight Plan, we started by using the Google Earth platform, in which the polygon of the area of interest was defined and sent for the DJI remote control. This file allows you to define the flight plan for the chosen area, based on the flight and capture parameters chosen.

Phase 2 – Realização do voo e recolha de dados

GCPs make an important role in georeferencing and

assessing the accuracy of the DSM model. Thus, before starting the flight, GCPs were marked in a distributed way in the terrain, with spray paint of color and size clearly visible. The coordinates of these points were measured with the help of the D-RTK 2, which must be connected to at least one of the GPS/GNSS Stations of the National Network of Permanent Stations GNSS (ReNEP), disseminated by the Directorate-General of the Territory and which defines the National Geodetic Reference.

The existence of the integrated GNSS navigation system and the IMU inertial system, together with the presence of the autopilot, allow the UAV to carry out the mission autonomously.

Phase 3 – Data Processing

To import the GCPs collected for the Pix4DMapper processing software it is necessary to transform the coordinates of these points to the desired reference system for the project. To perform the coordinates transformation, was used the tool available in mygeodata.cloud/cs2cs/.

The altitude obtained by the GNSS observations corresponds to the ellipsoidal height, that is, the height in relation to the geoid. So, to represent the data on a map, it is essential to determine the orthometric height that describes the height of the points on the earth's surface. For this, the NTv2 grid available in cgpr.dgterritorio.pt/webtranscoord/ was used.

To start the data processing step, a new project is created in Pix4DMapper, in which the images captured by the UAV are imported, as well as the respective central coordinates of each of the photos and orientations of the camera. The project output coordinates (ETRS89/PT-TM06) are defined as well as the vertical system (the Geoide Model EGM2008 is chosen, which will later be corrected for geodPT08 based on the coordinates entered in the GCPs).

During the first stage, the software uses the SfM technique to identify the homologous points in the images where there is overlap, allowing to find or optimize the position and orientation of the cameras and the internal orientation parameters, resulting from this step a cloud of sparse points, the positions and orientations of the cameras and the internal orientation parameters (Rodrigues, 2016)

After preprocessing, it is important to insert the coordinates of the GCPs in the software, and these should be marked in as many photographs as possible. The camera's internal and external orientation parameters are then reoptimized.

Later, the construction of the dense point cloud (and 3D textured mesh) is started, which allows the create of the DSM which in turn allows the orthophoto to be created. It is also possible to generate the digital terrain model (DTM) with information only of the elevation of the terrain, i.e., without the natural structures or built (after to make a classification of the point cloud), as well as the generation of level curves with information of the elevations of the respective models.

3. RESULTS AND DISCUSSIONS

3.1. Quarry mapping

To map the quarry, a flight was carried out covering an area of 105 064.2 m^2, at a height of 80 m relative to the take-off point, a flight speed of 6.3 m/s and a frontal and lateral overlap of 80%. The flight lasted approximately 55min and captured a total of 1418 images.

To correct the coordinates of the sparse point cloud (with 7 583 663 points) created in preprocessing (Figure 4) and increase the accuracy of the model, 4 GCPs were added. After re-optimizing the model, it is possible to increase the densification of the points of the same, by applying the Multi View Stereo algorithm (MVS), resulting in the dense point cloud with 46,7 times more points (353 910 040 points) than the previous cloud (Figure 5).

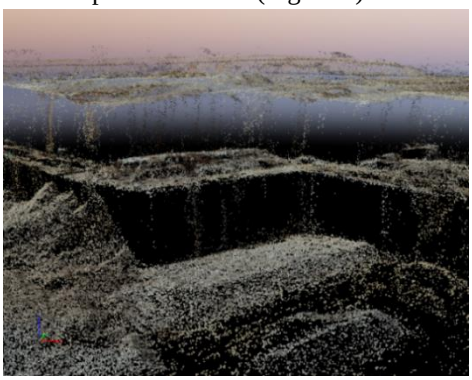

Figure 4: Sparse point cloud of a bench

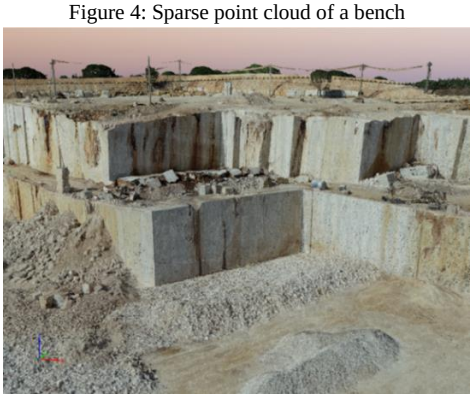

Figure 5: Dense point cloud of a bench

Once dense point clouds are generated, the application of interpolation and triangulation techniques is followed to produce the Digital Surface Model, the Digital Terrain Model and the Orthophoto (Figure 6).

3.1.1. Analysis of the use of GCPs

Table 2 shows the average RSME errors in georeferencing the final products of 5 flights, after the introduction of GCPs, as well as the translation made from the original data. The lowest RMSE value in georeferencing was verified with the flight in which a greater number of GCPs per flight area (GCPs/km2=16.8) was used, however,

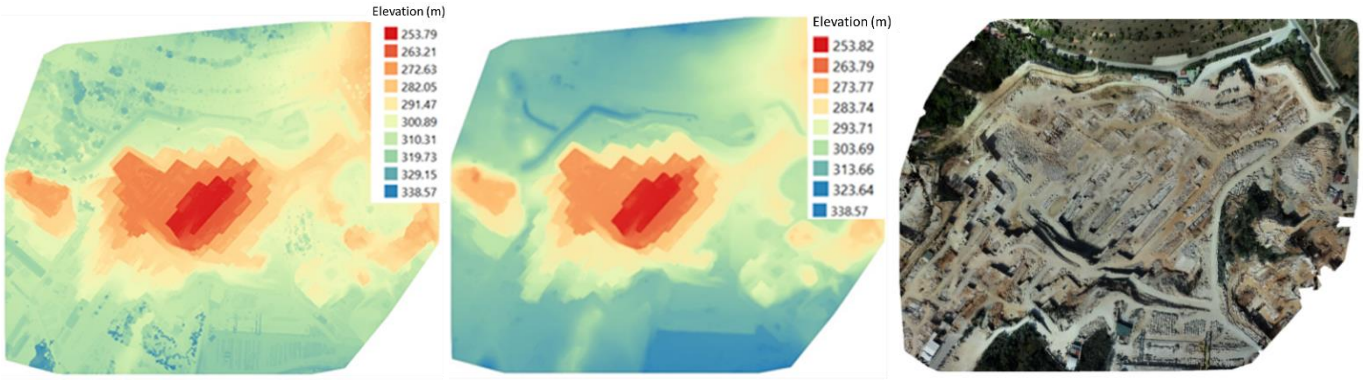

Figure 6: (a) Digital Surface Model, (b) Digital Terrain Model and (c) the Orthophoto

we can observe that a greater number of GCPs per area does not effectively correspond to a decrease in the error in georeferencing. We found that overall, the final products generated undergo a translation of the coordinates to the Northwest after the introduction of the control points in the project, with an average displacement of 0.411m to the west and 0.757m to the North, and a decrease in altitude with an average value of 0.373m.

Table 2: RMSE errors in georeferencing after the introduction of GCPs

				Translation		
Area [km2]	GCPs	GCPs/km2	RMSE[m]	X [m]	Y [m]	Z [m]
0,508	5	9,8	0,029	0,064	-1,131	-0,283
0,696	7	10,1	0,059	1,005	1,062	0,569
1,001	12	12,0	0,032	-0,476	0,424	-0,315
0,457	7	15,3	0,035	-0,016	0,367	-0,448
0,297	5	16,8	0,019	-0,496	0,804	-0,252
			0,035	0,411	0,757	0,373

3.1.2. Production support tool

One of the most important data for a good planning of the exploration of an ornamental rock quarry is the information of the respective work fronts. From the point cloud, as shown in Figure 44, it is possible to measure the length and height of each of the countertops, allowing to calculate the volume of each of the carvings to be disassembled. It is also possible to estimate the volume of each of the land and karst cavities present in the bench, to obtain the volume that corresponds only to the rock, calculate the actual density of the carving, and give an estimate of the utilization rate, that is, the volume of ornamental rock that is used considering quality factors and blockometry in relation to the total volume disassembled. This type of calculation is possible thanks to the speed of topographic surveys made using UAVs, which allow the updating of each front as the dismantling of the respective slabs is carried out. In addition to the dense point cloud, the creation of georeferenced orthophotos is a strong support tool not only in the planning of the dismantling but also in its monitoring and temporal recording, from the creation of detailed survey maps.

Figure 8 is a good example that illustrates these aspects, corresponding to a topographic survey carried out in October 2020, created with civil 3D software and in which the dismantling planning for that month, the registration of the felled slabs, the boundaries of the benches, the access ramps, the landscape recovery areas and all the quarry support infrastructures are designed.

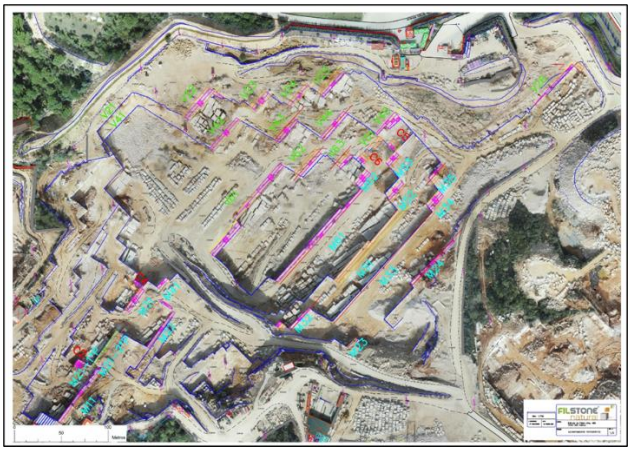

Figure 7: Topographic survey of the quarry (October 2020)

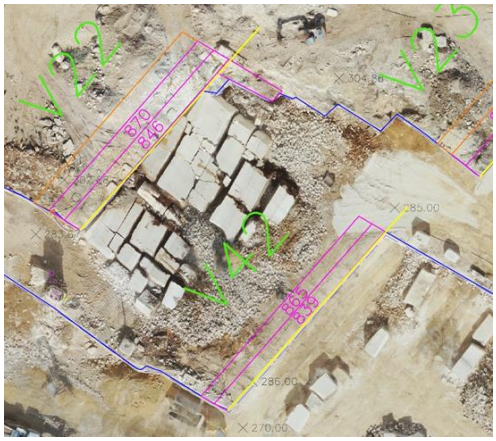

Figure 8: Zoom of topographic survey of the quarry (October 2020)

Figure 8 is an zoom of Figure 7, in which we can observe the planned slabs (orange sections) for each work front, the sections already felled from that planning (sections to purple) and their number of slab (reference number in order to store in a database all the information relating to that cut, from volumes, to the numbers of cut-off and thus, block

numbers and productions) as well as the direction of advancement of each front (yellow and red lines), which should always be perpendicular to the family of discontinuities in order to ensure the best use of the disassembled material.

The mapping of the quarry using unoccupied aerial vehicles also allows estimating the recovery rate of the cut, that is, calculating the volume of saleable material that is obtained by quartering the blocks existing in the volume used. To this end, a flight was made over a felled slab, having captured only 5 nadir photos (vertically) in manual flight.

Contrary to what was expected at the beginning of the development of this dissertation, it was not possible to distinguish through the images the types of mass of each of the fillets existing in the slab, since, being the masses distinguished by the dimension and dispersion of the grains in the rock matrix, it would be necessary for the drone to capture the images very close to the surface , in order to increase spatial resolution and it is possible to distinguish the particle size. Thus, the marking of the separation of the fillets, coincident with the cutting sites, and the identification of the type of mass was made manually on the ground and then made the photographic recording with the drone.

Figure 9 show the dashed marking of the division of the fillets and designation of the type of mass. Based on this marking, the volume of saleable material was made, and 346 t of the type of mass Beije ML and 66 t of the ML Mix mass were obtained.

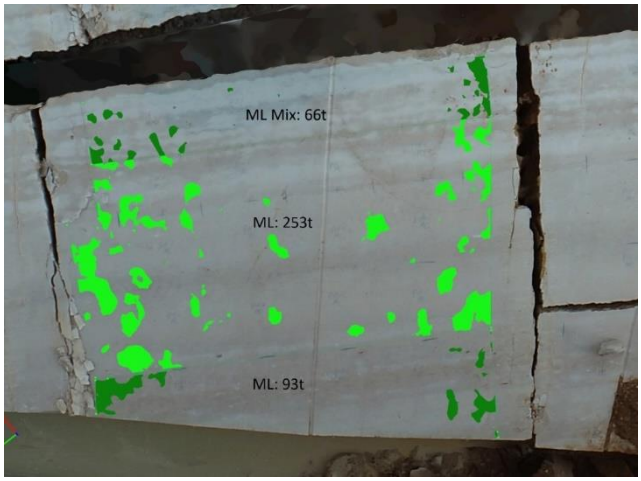

Figure 9: Division of the fillets and designation of the type of mass

In addition to the forecast of the saleable volume of the primary block, one can also make an analysis of the cuts of quartering and squaring and estimate the number of blocks that will result from this slab. So, by the observation of Figure 10 and based on the marking made on the ground, we can verify that, in the primary block in question, 3 cuts of mass separation will be made with a bench saw with a total of 29m linear (lines in red), and it is necessary that the retros make 1 cut of 9.5m (line to yellow) to complement the sectioning cuts. Subsequently, for the creation of the blocks it will be necessary that the retros make 5 cuts with a total of 36.7m (lines in blue), resulting in at least 16 marketable blocks.

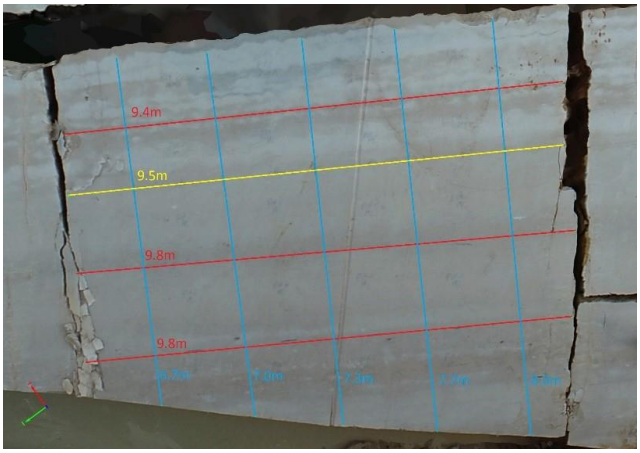

Figure 10: Quartering and squaring cuts of primary block

3.2. Volume measurement

3.2.1. Measuring the volume of aggregate piles

To measure the volume of aggregate stocks available in the crushing unit, a double grid flight was carried out with a coverage area of approximately 23.4 ha (234 000 m2), a duration of 32min and a total of 836 images. The flight was carried out at a height of 70m from the take-off point, at a flight speed of 4.2 m/s, a gimbal angle of 60º with the horizontal and a lateral and frontal overlap of 85%. Processing resulted in a GSD of 2.82cm/pixel and an RMS georeferencing error of 8mm. The generated point cloud has 192 972 938 points, with an average density of 376.7 points/m2, which contributes to an improvement in volume accuracy compared to classical methods, since the distance between interpolated points is much smaller. The digital terrain model features a GSD of 14.1cm/pixel (5 times the GSD value of the point cloud). After calibration of the captured images, tie points were created that allow, after placing the 3 measured control points on the ground, to recreate the dense point cloud (Figure 11).

Volume measurement was performed using the "Volumes" tool provided by Pix4DMapper that allows you to measure volumes of objects in a point cloud, based on the digital surface model. However, the dense point cloud has non-relevant objects that influence the calculation of, such as carrier screens and output cylinders of the product. In this way, before starting the measurement of the volume of stocks, it is necessary to filter the data from the point cloud to remove the undesirable structures. To this end, these points are marked in the point cloud and their classification is assigned (Figure 12), so that they are not used in stock volume calculations.

After the classification process, it was necessary to generate the DSM again so that in the volume measurement task, the volumes corresponding to undesirable objects were

not considered. Figure 13 corresponds to the digital surface model after the elimination of the transport screens.

Figure 11: Dense point cloud from crushing unit

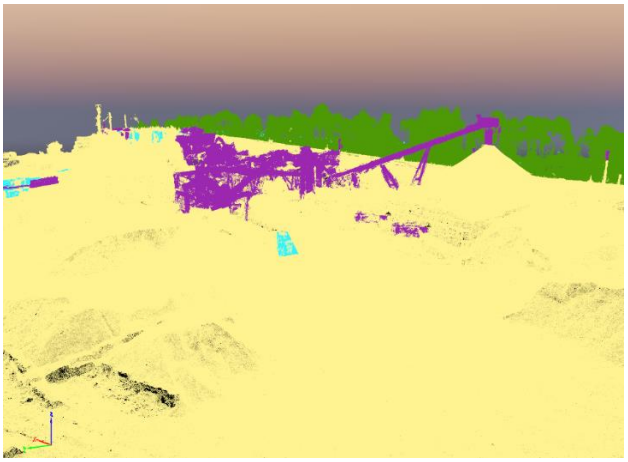

Figure 12: Dense point cloud classification

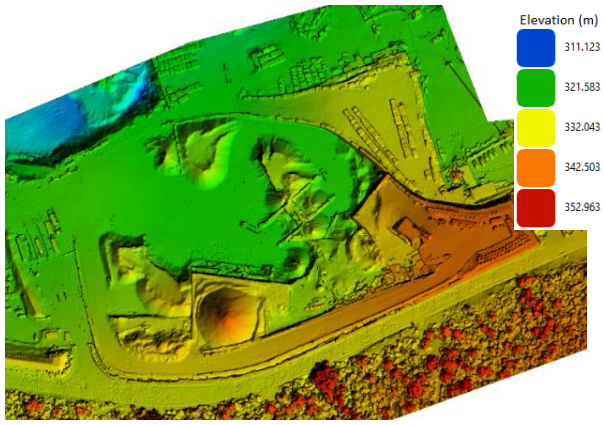

Figure 13: Digital surface model from after point cloud filtering

To measure the aggregate stocks (Figure 14), the perimeter of the pile to be measured was selected and the reference base was chosen as the lowest point of the surrounding floor (except for the 30/80mm gravel pile, the discharge of which is carried out directly into a box, as the reference base of the bottom of that storage box).

The images of unoccupied aerial vehicles can be used to generate point clouds and digital terrain models, to create a 3D reconstruction of the stockpiles with many points, allowing to make volume calculations with high accuracy, which was not possible with traditional methods due to the irregular shape of them. UAVs thus correspond to a fast and reliable tool for measuring and monitoring aggregate stocks, allowing you to conduct monthly or even weekly inventory reports and compare data over time.

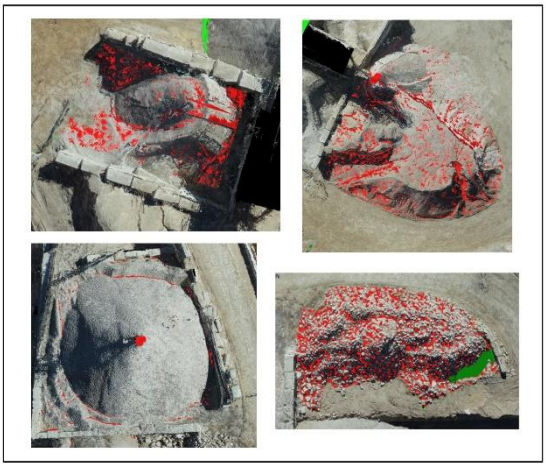

Figure 14: Stockpile volume measurement

3.2.2. Analysis of volume measurement capability

To study the reliability of volume calculation using UAV data, two analyses were performed, the first of a gravel stock, representing the case of an irregular volume, and the second of a row of blocks, representing the case of calculating volumes of regular objects.

Volume analysis - Gravel stack

Assuming that the gravel 30/80mm pile can be geometrically defined as an approximation to the volume of a cone, corresponding to the deposition pile of the material, and to a trapezoidal prism corresponding to the box, as shown in Figure 15, the volume of the cone was calculated, having obtained a volume of 8 748.5 m^3. The same volume was measured in the point cloud, using the Pix4DMapper software, which resulted in a volume of 9 027.7 m3, a difference of 0.6%. Thus, it can be considered that the measurement of volumes from the point cloud, obtained through the processing of images of UAVs, constitute a practical and reliable tool for the management of aggregate stocks.

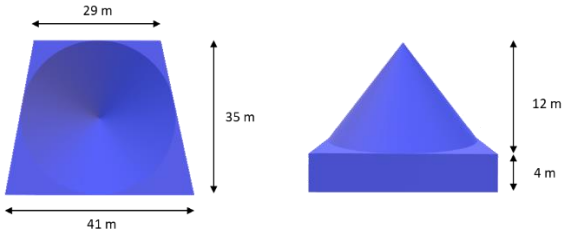

Figure 15: Geometrically approximation of gravel stockpile

Volume analysis - Block Park

For the second analysis of the volume calculation, a block park was surveyed, covering an area of 251 705.5 $m^{2,}$

with a duration of 39 min and 1 028 captured images. The flight was performed at 75 m height from the take-off point, at a flight speed of 5.9 m/s, an angle of the gimbal of 65º with the horizontal and a front and lateral overlap of 80%. From this survey, three rows were chosen, accounting for a total of 101 blocks and the measurement of volumes using pix4DMapper was performed (Figure 16).

From the volumes of the blocks obtained, their weight was calculated, multiplying the volume by the density of the limestone, having considered a value of 1.45 t/m^3. Then, the result obtained with the real weight of the blocks was compared. Table 3 shows that an absolute difference of 4% was obtained individually in two rows and 5% in a row. However, analyzing the data set of the 101 blocks, we obtained a difference of 2% between the weight obtained by measuring the volume of the point cloud and the real volume of the blocks, which allows us to conclude that the volume of objects from unoccupied aerial vehicles allows us to obtain very satisfactory results.

Figure 16: Measurement of ornamental blocks

Table 3: Absolute differences between the weight obtained by measuring the volume and the real weight of the blocks

	Weighing		Measurement	
Mass type	N. Blocks	Weight (t)	Weight of the Blocks (t)	Difference
Mix ML	34	512,86	490,52	4%
Blue ML	26	303,27	318,22	5%
Beije ML	41	449,92	429,92	4%
Total	101	1 266,05	1 238,65	2%

3.3. Study of the drainage network

Figure 17 corresponds to the digital surface model of the surrounding area of the garage, from which the digital terrain model was created (Figure 18).

As described in the methodology chapter, the first step to identify the drainage network is to define the direction of the water flow. Thus, the Flow Direction tool was applied, defined with the D8 algorithm to the digital terrain model and a map with the direction of water runoff was obtained, which then allows to determine the areas where there is greater or lesser flow accumulation (Figure 19). The red color in the figure represents the places where there is a higher probability for the flow of water, while the blue color identifies the areas where there is a low level of runoff. When compared to the digital terrain model, we can conclude that the places with the highest water flow correspond to the areas where there is a greater slope of the terrain.

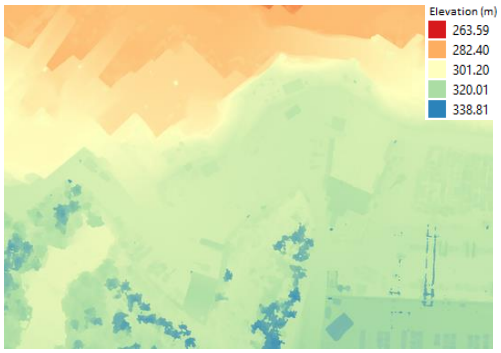

Figure 17: Digital surface model of the surrounding area of the garage

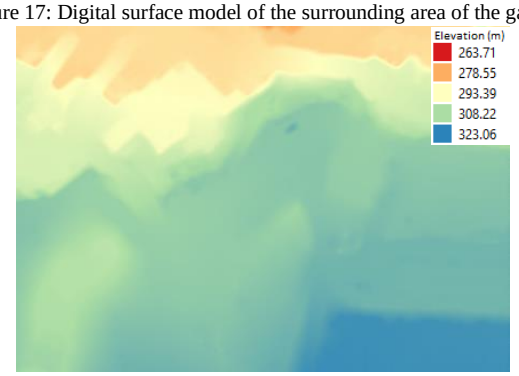

Figure 18: Digital terrain model of the surrounding area of the garage

The places where these water flows may be concentrated. To do this, the Flow Accumulation tool was applied and the places where the number of cells flowing to each adjacent cell was greater than 500 was calculated originating the drainage network of Figure 20.

By the observation of the Figure 20, we can observe that the main water drainage channels originate from the garage areas as well as the machine-washing zone located on the right side of garage 1, and the flow of water is routed by the topography of the land to the exploration area from the access ramps or the cliffs of the quarry boundary.

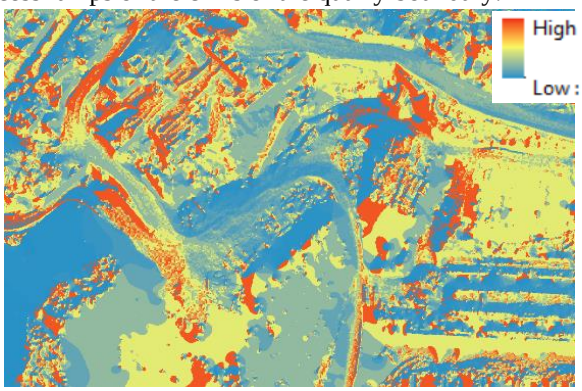

Figure 19: Flow direction map

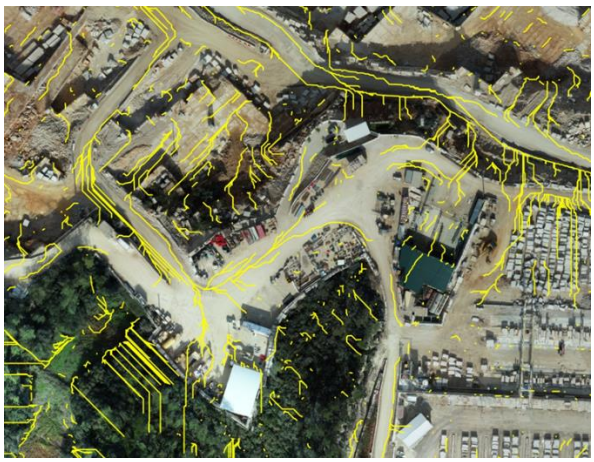

Figure 20: Drainage network

Garages and washing areas correspond to maintenance areas of machinery and equipment, in which waste is produced, such as used tires, scrap, waste oils, oil filters, lead batteries and materials contaminated with hydrocarbons, which must be managed and properly routed according to their level of danger to the environment. It is therefore necessary to ensure that there is no contamination of existing soil or water resources. To reduce the environmental impacts arising from the extractive industry, Filstone – Comércio de Rochas, S.A. is carrying out a project to build surface drainage ditches around the entire boundary to ensure the absence of rainwater run-out into it. The company is also paying special attention and developing a project for the construction of a hydrocarbon separator. Thus, all maintenance and washing tasks of equipment and machinery must be carried out on a waterproof floor, in which liquid effluents with hydrocarbons generated in the garages must be collected in a drainage system and driven to a hydrocarbon separator, which shall be cleaned periodically by a licensed entity. In the garage area, rainwater should also be sent to a hydrocarbon separator, the effluent of which is rejected in the decanting basin. The water stored in the decanting basin can be used in the processing area, in the cutting zone by wire saw machines, in which it is necessary to use water to perform the cuts.

3.4. Analysis of the influence of the extractive industry on vegetation - Casal Farto Extractive Nucleus

To evaluate the impact of the extractive activity of the quarry core in the surrounding environment, the temporal variation of the spectral signal of the vegetation cover was analyzed to determine the dust deposition. Different vegetation indices were tested based on RGB images, in two different time periods in which dust creation is quite distinct, one in a dry month, with little precipitation and high temperatures (end of September) and another in a humid month, with high precipitation and low temperatures (end of February). The RGB images (orthophotos) used for this study are shown in Figure 21, and the dust deposition site was highlighted next to the Fixed Crusher, at the bottom right of the images.

Figure 21:RGB images in September (left) and February (right)

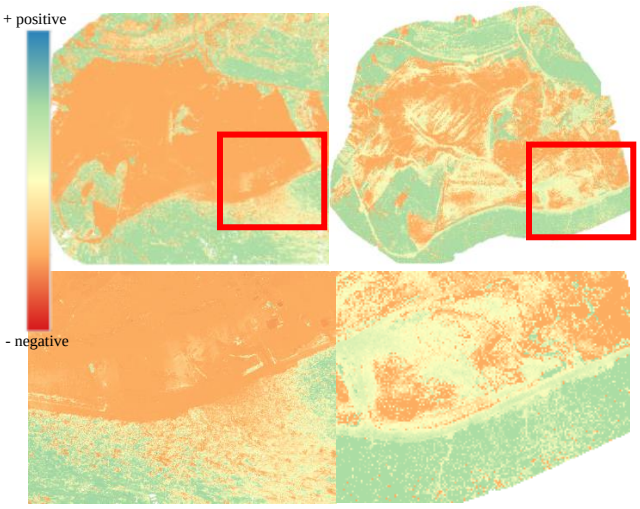

Figure 22: GLI index in September (left) and February (right) orthophotos

As mentioned in the methodology, 5 vegetation indexes based on RGB images were tested, but the index that obtained the best results was the GLI index so the calculation of this index for the rainy season was also performed.as shown in Figure 23. In the calculated images, the vegetation is represented in green (positive values of the index), while the soil is represented in orange (negative values of the index), and the areas with undergrowth are represented in yellow (intermediate/null values). Thus, the deposition of dust in the images is identified in yellow, in areas with low dust concentration, and orange in areas with higher dust concentration, and areas with zero concentration continue to be identified with green color, corresponding to the vegetation category. In the rainy season, some areas corresponding to the soil are also in yellow, possibly influenced by the accumulation of rainwater, so it can be concluded that the GLI index presents better results in the

distinction of vegetation and soil in periods of dry weather. However, the extensive dust deposition zone on the vegetation near the crushing unit in the dry period, represented orange and yellow, is notorious. On the other hand, it is possible to identify a decrease in the accumulation of dust near the crushing unit in wet weather periods, with the spatial increase of the positive values of the index and representing the vegetation areas.

To reduce the impact on the environment caused by the release of dust from the crushing unit, Filstone- Comércio de Rochas, S.A. is developing a project to encapsulate the crushing unit and the ensiling of industrial gravel.

The use of the unoccupied aerial vehicle, although equipped only with RGB camera in this work, proved to be once again a useful and easy-to-use tool in the inspection and evaluation of the impact of the extractive industry on the surrounding environment, in particular the places with higher dust deposition, which can be found from the spectral responses of vegetation cover.

4. CONCLUSIONS

From an operational point of view, the Phantom 4 RTK UAV used in this dissertation presented a good technical capacity to obtain field data in adequate quality and quantity, being easy to understand the procedures necessary to carry out the aerial surveys as well as their handling. Although the UAV has RTK technology, in which the coordinates of each image are corrected in real time, it is recommended to use control points on the ground to increase the accuracy and accuracy of the model.

As advantages of the use of UAEs in the extractive industry, in place of traditional methods, one can highlight the faster acquisition of data, combined with greater precision and creation of routines, which allow to support mining operations, enabling the decision-making well informed and faster.

About the specific objectives, it can be concluded that the use of UAV data is a strong tool for monitoring and planning the dismantling, through the creation of 3D models of the exploration area, allowing to calculate the dimensions and volume to be extracted on each work front, in addition to enabling the photographic recording of the usable volume and the cuts necessary for the completion of marketable blocks. However, contrary to what was expected at the beginning of the development of this dissertation, it was not possible to distinguish through the images the types of mass of each of the fillets existing in the carving, since, being the masses distinguished by the dimension and dispersion of the grains in the rock matrix, it would be necessary for the UAV to capture the images very close to the surface , in order to increase its spatial resolution and it is possible to distinguish the particle size.

About volume calculation, in particular the calculation of aggregate stocks, the use of UAV data in addition to increasing the accuracy of calculating battery volumes, also promotes increased safety of these tasks. Rapid data acquisition allows for more complete tracking of changes, allowing you to take volume measurements weekly or monthly to help you make better business decisions. Comparing the volume values obtained by the point cloud in the Pix4DMapper software and the mathematical model of the inert stack and the actual weight of the blocks arranged in the queues, a difference of 0.6% and 2% was obtained, respectively. We can thus conclude that images obtained using UAVs are a great tool for calculating volumes with high accuracy and reliability.

The high precision of the final products resulting from the processing of the UAV data also contribute to the study of the surface water drainage network, serving as a tool for the analysis and correction of the water flow routing, to avoid contamination of water or soil resources.

Finally, it can also be concluded that the images captured by the UAV are also a low-cost method for assessing the impact that the extractive industry has on the surrounding vegetation, from the calculation of vegetation indices based, in this case, on RGB images. It was concluded that the GLI vegetation index presented the best in the distinction between soil and vegetation, also allowing to identify the area of deposition and dispersion of dust resulting from the extractive industry. The calculation of the GLI index obtained better results in the distinction of vegetation and soil in the dry weather period. However, the index allowed identifying not only the place of deposition but also the decrease in the deposition area in the wet weather period.

We can conclude that the use of UAV data in the extractive industry allows to optimize the processes with greater agility, precision, safety, and economy, contributing to a better management of resources, anticipating situations and, thus, being able to strategically plan the decisions to be made, leaving with a photographic record and very detailed relief models of the entire area of interest and their involvement over time.

5. REFERENCES

AGISOFT LLC (2016). Agisoft PhotoScan User Manual - Professional Edition, Version 1.2 Consulted in 2020, September 7

Aguilera, D., Hernández, J., Taboada, J., Gonzálvez, P., López, D., García, B., Sanz, I., Perez, B., (2012) 3D Modelling and Accuracy Assessment of Granite Quarry using Unmmanned Aerial Vehicle. ISPRS Annals of the Photogrammetry, Remote Sensing and Spatial Information Sciences, Volume I-3

Arai, K., Shigetomi, O., Gondoh, K. & Miura, Y. (2016). Method for NIR Reflectance Estimation with Visible Camera Data based on Regression for NDVI Estimation and its Application for Insect Damage Detection of Rice Paddy

Fields. (IJARAI) International Journal of Advanced Research in Artificial Intelligence, 5(11), 17-22. Available at https://thesai.org/Downloads/IJARAI/Volume5No11/Paper_3-Method_for_NIR_Reflectance_Estimation_with_Visible_Camera_Data.pdf

Bemis, S., Micklethwaite, S., Turner, D., James, M., Akciz, S., Thiele, S. & Bangash, H. (2014). Ground-based and UAV-Based photogrammetry: A multi-scale, high-resolution mapping tool for Structural Geology and Paleoseismology. Journal of Structural Geology. 69. 163-178. doi: 10.1016/j.jsg.2014.10.007.

Bendig, J., Yu, K., Aasen, H., Bolten, A., Bennertz, S., Broscheit, J., Gnyp, M. & Bareth, G. (2015). Combining UAV-based plant height from crop surface models, visible, and near infrared vegetation indices for biomass monitoring in barley. International Journal of Applied Earth Observation and Geoinformation. 39. 79-87. doi: 10.1016/j.jag.2015.02.012.

Colomina, I. & Molina, P. (2014) Unmanned Aerial Systems for Photogrammetry and Remote Sensing: A Review. ISPRS Journal of Photogrammetry and Remote Sensing. 92. 79-97. doi: 10.1016/j.isprsjprs.2014.02.013

DroneShow. (2018). DJI anuncia o lançamento global do drone Phantom 4 RTK. Consulted in 2021, fevereiro 9 em https://droneshowla.com/dji-anuncia-o-lancamento-global-do-drone-phantom-4-rtk/

Gitelson, A., Kaufman, Y., Stark, R. & Rundquist, D. (2002). Novel Algorithms for Remote Estimation of Vegetation Fraction. Remote Sensing of Environment. 80. 76-87. doi: 10.1016/S0034-4257(01)00289-9.

Gunen, M. A., Taskanat, T., Atasever, O., & Besdok, E. (2019). Usage of Unmanned Aerial Vehicles (Uavs) in Determining Drainage Networks. E-journal of New World Sciences Academy, 14(1). doi: 10.12739/NWSA.2019.14.1.4A0062

Harwin, S. & Lucieer, A. (2012). Assessing the Accuracy of Georeferenced Point Clouds Produced via Multi-View Stereopsis from Unmanned Aerial Vehicle (UAV) Imagery. Remote Sensing. 4. 1573-1599. doi: 10.3390/rs4061573.

Krzystek, P. & Stuttgart. (1991). FULLY AUTOMATIC MEASUREMENT OF DIGITAL ELEVATION MODELS WITH MATCH-T. (Conference: 43rd Photogrammetric Week). Available at https://www.researchgate.net/publication/325113545_FULLY_AUTOMATIC_MEASUREMENT_OF_DIGITAL_ELEVATION_MODELS_WITH_MATCH-T

Lowe, D. G. (2004). Distinctive image features from scale-invariant keypoints. International journal of computer vision, 60(2):91–110. Zitiert auf Seite 46.

Raeva, P. L., Filipova, S. L., & Filipov, D. G. (2016). Volume computation of a stockpile - A study case comparing GPS and uav measurements in an open pit quarry. International Archives of the Photogrammetry, Remote Sensing and Spatial Information Sciences - ISPRS Archives, 2016-January. doi: 10.5194/isprsarchives-XLI-B1-999-2016

ReNEP. (n.d.). Consulted in 2021, June 13 at https://renep.dgterritorio.gov.pt/

Rouse, J.W., R.H. Haas, J.A. Schell, and D.W. Deering (1974). Monitoring vegetation systems in the Great Plains with ERTS. Third Earth Resources Technology Satellite–1 Syposium. 1. 309-317. Available at SNWA_Exh_586_Rouse 1974.pdf (nv.gov)

Salvini, R., Mastrorocco, G., Seddaiu, M., Rossi, D., & Vanneschi, C. (2017). The use of an unmanned aerial vehicle for fracture mapping within a marble quarry (Carrara, Italy): photogrammetry and discrete fracture network modelling. Geomatics, Natural Hazards and Risk, 8(1). doi: 10.1080/19475705.2016.1199053

Szeliski, R. (2010). Computer Vision: Algorithms and Applications. Available at https://szeliski.org/Book/drafts/SzeliskiBook_20100903_draft.pdf

Tucker, C.J., (1979). Red and photographic infrared linear combinations for monitoring vegetation. Remote Sens. Environ. 8, 127–150, doi:10.1016/0034-4257(79) 90,013-0

Vasconcelos, S. L., Souza, J. C., Rocha, S. S., Rodrigues, H. C., Maris, J. L., & Silva, R. F. (2018). Determinação de volumes e áreas em mineração a céu aberto utilizando drones. 9° Congresso Brasileiro de Minas a Céu Aberto e Minas Subterrâneas. Available at https://www.researchgate.net/publication/337951370